Ocean Engineering 247 (2022) 110516

Contents lists available at ScienceDirect

Ocean Engineering

journal homepage: www.elsevier.com/locate/oceaneng

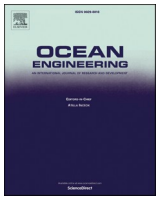

Active disturbance rejection control for ship path following with Euler method

Hugan Zhang, Xianku Zhang *, Tian Cao, Renxiang Bu

Navigation College, Dalian Maritime University, Liaoning, 116026, China

ARTICLE INFO

Keywords:
Ship motion control
ADRC
Path following
Position prediction
Euler method

ABSTRACT

In order to solve the problems of uncertain model, unknown disturbances and overshoot in the process of ship path following, an active disturbance rejection control (ADRC) for ship path following with Euler method is proposed. Firstly, the virtual heading angle is designed by backstepping algorithm, and the three degree of freedom position control is transformed into one degree of freedom heading control. Due to the characteristics of large inertia and large time delay in ship path following, the overshoot is easy to occur in the process of path following. Euler method is used to predict the future position in order to reduce the overshoot in the process of path following. To solve the problems of internal model uncertainty and external disturbances such as wind, waves and currents, the power expended state observer is used to observe and compensate it to the controller. It has higher observation accuracy without changing the observer parameters. Finally, the simulation results show the effectiveness of the designed controller.

1. Introduction

Underactuated ship path following is a typical motion control problem because the ship lacks lateral control input. The ship was strongly affected by the perturbation of hydrodynamic coefficients and external disturbances such as wind, waves and currents in actual navigation. Therefore, a controller suitable for underactuated ship motion in this environment was designed with certain difficulties. In(Li et al., 2013),a composite control method of ADRC and sliding mode were proposed to overcome the error interference caused by external disturbances. However many times this special environmental disturbances was unknown, In (Zhu and Du, 2020) the compounded uncertain term caused by the unknown parameters and disturbances was transformed into a linear parametric form with a single parameter called virtual parameter. Then, a novel robust adaptive ship trajectory tracking control law was designed using the adaptive vector-backstepping design method. On the other hand, Kinematic uncertainty and environmental disturbances for underactuated ships, In (Sun, 2017) a novel nonlinear robust adaptive scheme with sliding mode control was proposed for underactuated ships to track the desired path generated by the logical virtual ship in the presence of unknown plant parameters and environmental disturbances (Dai et al., 2019). proposed an adaptive neural tracking control method for underactuated surface ships with model uncertainty and time-varying external disturbances. The neural network approximator was used to approximate the uncertain ship dynamics, and the disturbance observer was proposed to estimate the unknown disturbances. In (Shojaei, 2015), a radial basis function neural network and adaptive robust control technology were used to maintain the robustness of the controller to unmodeled dynamics and environmental disturbances caused by waves and ocean currents (Guerrero et al., 2019). had mainly studied the design of adaptive high-order sliding mode control for trajectory tracking of underwater vehicles. This control law retains the advantages of robust control, does not need to know the upper bound of the disturbances, and was easy to tune in practical applications. And in (Chwa, 2021) an adaptive neural output feedback tracking control method was proposed.

Due to the strong nonlinearity, uncertainty and dynamic constraints of ship motion, designing a high-performance ship heading controller was still a challenging task, such as Non-linear feedback controller (Zhang et al., 2019),(Zhao et al., 2019), sliding mode control(Moradi and Malekizade, 2013),(Perera and Guedes Soares, 2012),(Esfahani et al., 2019), (Li et al., 2018) model predictive control (Mizuno et al., 2016),(Yang et al., 2020),(Guerrero et al., 2019)adaptive control (Nguyen et al., 2019),(Kurtoglu et al., 2021),(Wang et al., 2021). Neural network control(Guan et al., 2019),(Le, 2021),and so on. In the study of underactuated ship path following control problem. In(Do and Pan,

* Corresponding author.
E-mail address: zhangxk@dlmu.edu.cn (X. Zhang).

https://doi.org/10.1016/j.oceaneng.2021.110516
Received 9 October 2021; Received in revised form 13 December 2021; Accepted 30 December 2021
Available online 21 February 2022

2006), a new design method of global controller was proposed. The controller can make the under-driven ship move along the reference path under the disturbances. However, the controller does not consider the saturation surge force and transverse pendulum moment(Zhang et al., 2015). used dynamic surface control (DSC) technology, neural network approximation and polar coordinate schemes, a practical adaptive neural control algorithm was proposed. This algorithm can eliminate the need for hydrodynamic damping structures and precise information about ocean disturbances. In order to further reduce the multi-dimensional path following error of underactuated ships (Zhang et al., 2021c), proposed a three-dimensional path following control scheme based on adaptive approach angle, which converts the three-dimensional tracking error into heading angle and elevation angle tracking error, and then designed the motion control law based on Lyapunov theory and backstepping technology. In order to simplify its control difficulty(Lekkas and Fossen, 2014), , (Moreira et al., 2007)used line of sight (LOS) to convert three-dimensional path following into one-dimensional course control. In (Liu et al., 2016)a new predictor-based under-actuated surface vehicle path tracking line of sight (PLOS) guidance law was proposed. The proposed guidance law not only maintains the simplicity of classic LOS guidance, but also can identify the vehicle sideslip angle smoothly and quickly. Also (Huang and Fan, 2017) ADRC heading keeping controllers were used to identify environmental disturbances and model parameter disturbances. An improved adaptive line of sight (ALOS) guidance method is proposed to track the reference path(Min and Zhang, 2021). the basis of conventional LOS guidance, further improvements were made. Three technologies including nonlinear sideslip angle observer, time-varying forward-looking distance, and new advance turning distance were introduced, and a multi-technology was proposed. Improved line-of-sight MILOS guidance, more likely to be directly used in navigation practice. On the basis of the above research, this paper proposes a new active disturbance rejection control for ship path following with Euler method. The main contributions of this paper are as follows:

(1) Through the real ship experimental data, it is verified that the design model has certain accuracy.
(2) The three degree of freedom path following is transformed into one degree of freedom heading control by backstepping algorithm. The future position is predicted by Euler method to reduce the overshoot in the process of path following.
(3) The power function is used to improve the extended state observer. When the error is too large, the error gain will decrease and when the error is too small, the error gain will increase, which improves the accuracy of the observer.

The paper is constructed as follows: Firstly, Section 1 introduces the mathematical model of ship motion, including the simulation model and design model. And the simulation model is verified. Next, Section 2 describes the design process of the ship motion controller, including backstepping, Euler method, and ADRC. Then, Section 3 presents numerical simulation results. Finally, Section 4 provides the conclusions of this paper.

2. Ship motion model

2.1. Simulation model

MMG model is one of the solutions for ship maneuvering motion simulations developed in Japan. The model was proposed by a research group called Maneuvering Modeling Group (MMG) in Japanese Towing Tank Conference (JTTC), and the outline was reported in the Bulletin of Society of Naval Architects of Japan in 1977.(Yasukawa and Yoshimura, 2015). In this paper, MMG model is used to simulate the ship path following.

$$\begin{cases} \dot{x} = u\cos\psi - v\sin\psi = \sqrt{u^2+v^2}\cos(\psi+\beta) \\ \dot{y} = u\sin\psi + \cos\psi = \sqrt{u^2+v^2}\sin(\psi+\beta) \\ \dot{\psi} = r \\ \dot{u} = \begin{bmatrix} (m+m_y)vr + X_H + X_P + X_W + X_{WAVE} \\ +(m_x - m_y)V_c\sin(\psi_c - \psi)r \end{bmatrix} / (m+m_x) \\ \dot{v} = \begin{bmatrix} (m+m_x)ur + Y_H + Y_P + Y_W + Y_{WAVE} \\ +(m_x - m_y)V_c\cos(\psi_c - \psi)r \end{bmatrix} / (m+m_y) \\ \dot{r} = (N_H + N_P + N_R + N_W + N_{WAVE}) / (I_{ZZ} + J_{ZZ}) \end{cases} \tag{1}$$

In Eq. (1), m is the mass of the ship, m_x and m_y are added mass, X_H、Y_H and N_H are naked hull, X_P、Y_P and N_P are propeller force (moment), ψ_c and V_c are flow direction and velocity respectively, X_W、Y_W and N_W are wind force (moment), X_{Wave}、Y_{Wave} and N_{Wave} are wave force (moment), I_{zz} is the moment of inertia of the ship around the vertical axis, J_{zz} is additional moment of inertia, and X_R、Y_R and N_R are rudder force (moment), which are calculated as follows(Zongxuan et al., 2021):

$$\begin{cases} X_R = -(1-t_R)F_N\sin\delta \\ Y_R = -(1+a_H)F_N\cos\delta \\ N_R = -(x_R + a_H x_H)F_N\cos\delta \end{cases} \tag{2}$$

In Eq. (2), t_R is the reduction of rudder resistance, α_H is the ratio of additional lateral force caused by rudder and rudder lateral force, x_H is the distance from the center of action of lateral force induced by rudder to the center of gravity of ship, F_N is the positive pressure of rudder.

2.2. Design model

Path following does not need to consider the time factor, so in this paper, the propeller speed is set as a fixed value, only considering the rudder angle input. Then Eq. (1) can be simplified as the design model of Eq. (3)(Li et al., 2020).

$$\begin{cases} \dot{x} = u\cos\psi - v\sin\psi = \sqrt{u^2+v^2}\cos(\psi+\beta) \\ \dot{y} = u\sin\psi + v\cos\psi = \sqrt{u^2+v^2}\sin(\psi+\beta) \\ \dot{\psi} = r \\ \dot{r} = -\dfrac{r}{T} + \dfrac{K}{T}\delta + f \\ \beta = \arctan(v/u) \\ f = f_1 + d \end{cases} \tag{3}$$

In Eq. (3), K is the turning ability index, T is the turning lag index, f_1 is the internal model uncertainty, d is the external disturbances uncertainty, and f is the sum of the model uncertainty f_1 and external disturbances d, that is, the total unknown term.

Assumption 1: f is an unknown and bounded value, and does not change dramatically over time, namely $f \le f_{max}$ and $\dot{f}$ is a small value.

*Remark*1 : f boundedness is a necessary condition for the system to be controllable. If the unknown term f is unbounded, the designed controller is meaningless. In addition, the environment changes slowly during the movement of the ship, so $\dot{f}$ is a small value, which is in line with the actual navigation.

2.3. Model validation

In order to verify the effectiveness of the model, the model is verified by comparing the real ship data with the simulation data, and the real ship experiment is carried out with the Yupeng vessel of Dalian Maritime University. Fig. 1 shows the sea experiments of Yupeng vessel, and the comparison of the simulation experiments of Nomoto model. In order to conform to the navigation practice, the rudder servo system is added in the model simulation, and the maximum rudder angle is limited to 0 ±

Fig. 1. Scene of Yupeng vessel 's real ship experiment.

35°, The maximum rudder speed is limited to ±5°/s. The average wind direction is 3°, The relative wind speed is 10.1 m/s, and 35°right rudder rotation test is carry out with wind. In order to quantify the approximation degree of the model, Eq. (4) is defined

$$\text{Conformity} = \left(1 - \frac{|C_s - C_t|}{C_t}\right) \times 100\% \tag{4}$$

In Eq. (4),C_s is the simulation test value, C_t is the real ship test value. Fig. 2 compares the cycle radius of the real ship experiment and the simulation experiment at the right rudder 35° cycle. the accuracy of Yupeng vessel is 87%. Fig. 3 shows the effect of 10°/10° Z-shaped test. Because the speed reduction is small during the 10°/10° Z-shaped test, the change of speed is ignored. ψ For the ship course, in the real ship experiment, the first overtaking angle is 4.3°, the second overtaking angle is 8.9°, in the simulation experiment, the first overtaking angle is 5.2°, the second overtaking angle is 10.4°, and the accuracy is 79% and 83% respectively. This meets the accuracy requirements of the ship model.

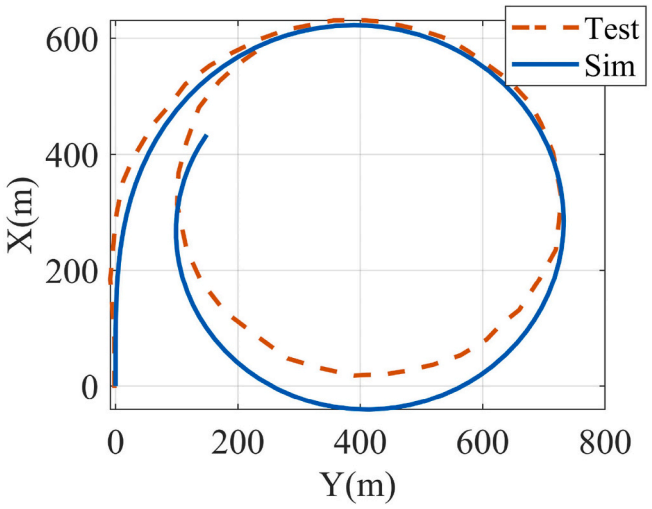

Fig. 2. Comparison between simulation and real ship experiment when turning right 35°

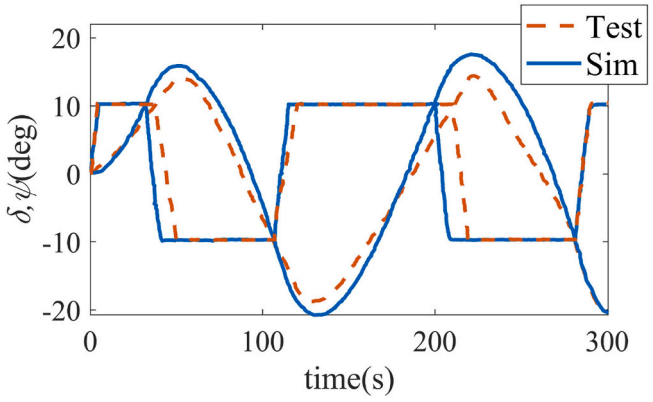

Fig. 3. Comparison between simulation and real ship experiment when 10°/10° Z-shaped test.

3. Path following controller

In this paper, the path following controller consists of two parts. The first part is to design the virtual heading angle based on the predicted future error and backstepping algorithm; the second part is to use the ADRC to realize the heading control.

3.1. Backstepping algorithm

This section uses the backstepping algorithm to design the virtual heading angle according to the predicted future error. Firstly, the derivation of the lateral displacement deviation $y_e = y - y_d$ is obtained, and the Eq. (3) is substituted by:

$$\begin{aligned} \dot{y}_e &= \dot{y} - \dot{y}_d \\ &= \sqrt{u^2 + v^2}\sin(\psi + \beta) - \frac{dy_d}{dx}\cdot\frac{dx}{dt} \\ &= \sqrt{u^2 + v^2}\sin(\psi + \beta) - \frac{dy_d}{dx}\sqrt{u^2 + v^2}\cos(\psi + \beta) \\ &= \sqrt{u^2 + v^2}\sin(\psi + \beta - \theta) \end{aligned} \tag{5}$$

In Eq (5), θ is the slope of the reference path. According to Eq. (5), design virtual heading:

$$\psi_d = -c_0 \tanh(c_1 y_e) - \beta + \theta \tag{6}$$

In Eq. (6), c_0 and c_1 are positive design parameters respectively, the Lyapunov function $V_1 = (1/2)\ y_e{}^2$ is selected and its derivative is obtained

$$\begin{aligned} \dot{V}_1 &= y_e \dot{y}_e \\ &= y_e\sqrt{u^2 + v^2}\sin((-c_0 \tanh(c_1 y_e) - \beta + \theta) + \beta - \theta) \\ &= -y_e\sqrt{u^2 + v^2}\sin(c_0 \tanh(c_1 y_e)) \end{aligned} \tag{7}$$

In Eq. (7), the value of $c_0\tanh(c_1 y_e)$ is between $(-\pi/3, \pi/3)$, $\sin(c_0\tanh(c_1 y_e))$ is an odd function, and the sign are the same as y_e. It can be obtained $-y_e\sqrt{u^2 + v^2}\sin(c_0 \tanh(c_1 y_e)) \le 0$, thus $\dot{V}_1 \le 0$. Therefore, the designed reference course Eq. (6) can make the path deviation tend to 0.

However, due to the large inertia and large time delay of ship motion, it is easy to overshoot in the process of path following. In order to solve the overshoot phenomenon in the process of ship path following, the future position is predicted by Euler method, and the current and future course deviation is considered. In this way, the ship can predict the path in advance, so as to turn as soon as possible and avoid over-

shoot. Firstly, according to Eq. (3) and Euler method, all ship positions in the future time domain n are predicted (Zhang et al., 2021a).

$$\begin{cases} \bar{y}(k+1) = y(k) + \sum_{j=0}^{0} T_1 \dot{y}(k+j) \\ \bar{y}(k+2) = y(k) + \sum_{j=0}^{1} T_1 \dot{y}(k+j) \\ \bar{y}(k+3) = y(k) + \sum_{j=0}^{2} T_1 \dot{y}(k+j) \\ \cdots \\ \bar{y}(k+n) = y(k) + \sum_{j=0}^{n-1} T_1 \dot{y}(k+j) \end{cases} \tag{8}$$

In Eq. (8), $\bar{y}$ $(k+n)$ is the predicted value of y at $k+n$, t is the predicted sampling time, and $\dot{y}$ (k) is the discretization result of the second term in Eq. (3).

$$\dot{y}(k) = u(k)\sin\psi(k) + v(k)\cos\psi(k) \tag{9}$$

The future error y $(k+j), j = 1, 2, \ldots n$ is calculated by the predicted value of Eq. (8) and reference path y_d, n is as follows:

$$\begin{cases} \bar{e}_y(k+1) = \bar{y}(k+1) - y_d(k+1) \\ \bar{e}_y(k+2) = \bar{y}(k+2) - y_d(k+2) \\ \bar{e}_y(k+3) = \bar{y}(k+3) - y_d(k+3) \\ \vdots \\ \bar{e}_y(k+n) = \bar{y}(k+n) - y_d(k+n) \end{cases} \tag{10}$$

According to Eq. (10), the total path error including current time and future time is constructed as follows:

$$y_E(y, y_d) = P\bar{e}_y(k) + \sum_{j=1}^{n} Q\bar{e}_y(k+j) \tag{11}$$

In Eq. (11) P and Q are weights to adjust the balance between current time error and future error. According to Eq. (11), the virtual heading course is designed as follows:

$$\psi_d = -c_1 \tanh(c_0 y_E) - \beta + \theta \tag{12}$$

3.2. Design of LESO

The extended state observer is the core of ADRC structure. Its basic idea is to estimate and compensate the uncertain dynamic in real time and compensate in feedback control. The uncertain disturbances that can be estimated whatever time-varying and time invariant, linear and nonlinear, internal and external disturbances. The earliest ESO is composed of fhan function. When the error is small, it has nonlinear property, when the error is large, it has linear property. However, due to its complex parameter adjustment and non differentiable points, the concept of bandwidth was proposed in reference(Gao, 2003), which linearized the state observer and effectively solved the problem of observer parameter adjustment. LESO has the characteristics of convenient parameter adjustment, but it also reduces the accuracy of the observer to a certain extent.

Firstly, LESO is used to estimate the total unknown term f and the yaw rate r in heading control. The LESO of the second order system is designed as follows:

$$\begin{cases} \dot{\hat{\psi}} = \hat{r} - k_1(\hat{\psi} - \psi) \\ \dot{\hat{r}} = f - k_2(\hat{\psi} - \psi) + \frac{K}{T}\delta - \frac{\hat{r}}{T} \\ \hat{f} = -k_3(\hat{\psi} - \psi) \\ y_1 = \hat{r} \\ y_2 = \hat{f} \end{cases} \tag{13}$$

In order to improve the accuracy of the LESO, there is a large gain when the error is small and a small gain when the error is large. The power function is used instead of the linear function.

Without changing the parameters of the original observer, the improved observer is as follows

$$\begin{cases} \dot{\hat{\psi}} = \hat{r} - k_1(\hat{\psi} - \psi)^{1/3} \\ \dot{\hat{r}} = f - k_2(\hat{\psi} - \psi)^{1/3} + \frac{K}{T}\delta - \frac{\hat{r}}{T} \\ \dot{\hat{f}} = -k_3(\hat{\psi} - \psi)^{1/3} \\ y_1 = \hat{r} \\ y_2 = \hat{f} \end{cases} \tag{14}$$

In Eq (14) , $\hat{\psi}$、 $\hat{r}$、 $\hat{f}$ are the estimated value of ψ、r、 f respectively , k1、k_2、k_3 are the parameters based on observer bandwidth, it is used to adjust the feedback gain of estimation error. The input of ESO are δ andψ,and the output are $\hat{f}$ and $\hat{r}$. the estimation value is defined.

$$\begin{cases} \tilde{\psi} = \hat{\psi} - \psi \\ \tilde{r} = \hat{r} - r \\ \tilde{f} = \hat{f} - f \end{cases} \tag{15}$$

The estimated error is calculated as follows:

$$\begin{cases} \dot{\tilde{\psi}} = \tilde{r} - k_1\tilde{\psi}^{1/3} \\ \dot{\tilde{r}} = \tilde{f} - k_2\tilde{\psi}^{1/3} - \frac{\tilde{r}}{T} \\ \dot{\tilde{f}} = -k_3\tilde{\psi}^{1/3} - \dot{f} \end{cases} \tag{16}$$

Select Lyapunov function $V2$ as follows:

$$V_2 = \frac{3}{4}\tilde{\psi}^{4/3} + \frac{1}{2}\chi\tilde{r}^2 + \frac{1}{2}\zeta\tilde{f}^2 \tag{17}$$

Find the time derivative of V_2 and substitute it into the estimation error

$$\begin{aligned} V_2 &= \tilde{\psi}^{1/3}\dot{\tilde{\psi}} + \chi\tilde{r}\dot{\tilde{r}} + \zeta\tilde{f}\dot{\tilde{f}} \\ &= \tilde{\psi}^{1/3}\left(\tilde{r} - k_1\tilde{\psi}^{1/3}\right) + \chi\tilde{r}\left(\tilde{f} - k_2\tilde{\psi}^{1/3} - \frac{\tilde{r}}{T}\right) + \zeta\tilde{f}\left(-k_3\tilde{\psi}^{1/3} - \dot{f}\right) \\ &= -k_1\tilde{\psi}^{2/3} - \chi\frac{\tilde{r}^2}{T} + \tilde{\psi}^{1/3}\tilde{r}(1 - \chi k_2) + \tilde{f}\left(\chi\tilde{r} - k_3\zeta\tilde{\psi}^{1/3}\right) - \zeta\tilde{f}\dot{f} \end{aligned} \tag{18}$$

For the convenience of analysis, variables z_1, z_2 and z_3 are introduced to simplify the above equation as follows:

$$\begin{cases} V_2 = -k_1\tilde{\psi}^{2/3} - \chi\frac{\tilde{r}^2}{T} + z_1 + z_2 + z_3 \\ z_1 = \tilde{\psi}^{1/3}\tilde{r}(1 - \chi k_2) \\ z_2 = \tilde{f}\left(\chi\tilde{r} - k_3\zeta\tilde{\psi}^{1/3}\right) \\ z_3 = -\zeta\tilde{f}\dot{f} \end{cases} \tag{19}$$

Select appropriate parameters $\chi = 1/k_2$,we can get $z_1 = 0$. Consider the Assumption 1 , z_3 is bounded and small. A modification of the first term of Eq. (16) can be obtained

$$\tilde{r} = \dot{\tilde{\psi}} + k_1\tilde{\psi}^{1/3} \tag{20}$$

Bring z_2 into Eq. (20) to obtain

$$\begin{aligned} z_2 &= \tilde{f}\left(\chi\left(\dot{\tilde{\psi}} + k_1\tilde{\psi}^{1/3}\right) - k_3\zeta\tilde{\psi}^{1/3}\right) \\ &= \tilde{f}\chi\dot{\tilde{\psi}} + \tilde{f}\chi k_1\tilde{\psi}^{1/3} - \tilde{f}k_3\zeta\tilde{\psi}^{1/3} \\ &= \tilde{f}\chi\dot{\tilde{\psi}} + \tilde{f}\tilde{\psi}^{1/3}(\chi k_1 - k_3\zeta) \end{aligned} \tag{21}$$

In Eq (21) , Select the appropriate parameter relationship, $\zeta = k_1\chi/k_3$, We can make the second term equal to 0, Consider the derivative principle: when the derivative of a function is greater than/less than 0, its corresponding function value will always increase/decrease. When $\dot{\tilde{\psi}} < 0$,$\tilde{\psi}$ will decrease, to$\tilde{\psi} < 0$, so$\dot{\tilde{f}} > 0$,$\tilde{f}$ will also increase until $\tilde{f} > 0$ so we can get $z_2 < 0$,on the other hand, when $\dot{\tilde{\psi}} > 0$, $\tilde{\psi}$ will increase

to $\widetilde{\psi} > 0$,so $\dot{\widetilde{f}} < 0$,we also can get $z_2 < 0$. So there is a small positive number Ω,can make $z_1 + z_2 + z_3 \leq \Omega$.

At this point, the derivative of V_2 over time can be rearranged as

$$\begin{cases} V_2 = -k_1\widetilde{\psi}^{2/3} - \chi\dfrac{\widetilde{r}^2}{T} + z_1 + z_2 + z_3 \leq -\widetilde{e} + \Omega \\ \widetilde{e} = k_1\widetilde{\psi}^{2/3} + \chi\dfrac{\widetilde{r}^2}{T} \end{cases} \tag{22}$$

In Eq (22), $\widetilde{e} \geq 0$ is the quadratic term of the estimation error. So when $-\widetilde{e} + \Omega < 0$, Then the derivative of V_2 is less than 0, that is, the system is stable; At the same time, when $-\widetilde{e} + \Omega > 0$, so $\widetilde{e} < \Omega$, $\widetilde{e}$ will be constrained to a range less than Ω. Then the system is stable in the sense of Lyapunov. That is, the established heading system PESO can estimate the unknown term f and yaw rate r.

3.3. The linear state error feedback law

Once the observer is designed and bandwidth is well tuned, its outputs will track ψ,r and f respectively. The PD control law is taken as:

$$\begin{aligned} u_1 &= -K_p\cdot(\widehat{\psi} - \psi_d) - K_d\cdot(\dot{\psi} - \dot{\psi}_d) \\ &= -K_p\cdot\psi_e - K_d\cdot\dot{\psi}_e \end{aligned} \tag{23}$$

In Eq. (23) K_p and K_d are the parameters of controller gain; $\psi_e = \widehat{\psi} - \psi_d$ is heading deviation. Then the final error feedback control law is (Zhang et al., 2021b):

$$\delta = \frac{T}{K}(u_1 - \widehat{f}) \tag{24}$$

4. Simulation of ship path following control

In order to verify the effectiveness of the designed controller, comparative simulation experiments are carried out. The MMG model in Eq. (1) is taken as the simulation model. The parameters of "Yupeng" are shown in Table 1.

The wind force (moment) X_w、 Y_w and N_w in Eq. (1) are calculated as follows(Wang et al., 2018):

$$\begin{cases} X_w = -\dfrac{1}{2}\rho_a A_f U_R^2 C_{wx}(\alpha_R) \\ Y_w = \dfrac{1}{2}\rho_a A_s U_R^2 C_{wy}(\alpha_R) \\ N_w = -\dfrac{1}{2}\rho_a A_s L_{oa} U_R^2 C_{wn}(\alpha_R) \end{cases} \tag{25}$$

In Eq. (25), ρ_α is the air density, α_R is the relative wind direction angle, U_R is the relative wind speed, A_f and A_s are the forward projection area and side projection area above the waterline of the ship, $L_{o\alpha}$ is the total length of the ship, $C_{Xw}(\lambda)$、$C_{Yw}(\lambda)$ and $C_{Nw}(\lambda)$ are the wind pressure (moment) coefficients respectively.

Since large ships can resist the first-order wave disturbances in their navigation, this paper only considers the second-order wave disturbances, and the wave forces (moments) X_{wave}, Y_{wave} and N_{wave} are calculated as follows (Xiaobin et al., 2016)

$$\begin{cases} X_{wave} = \dfrac{1}{2}\rho L\alpha^2 \cos\chi C_{Xw}(\lambda) \\ Y_{wave} = \dfrac{1}{2}\rho L\alpha^2 \sin\chi C_{Yw}(\lambda) \\ N_{wave} = \dfrac{1}{2}\rho L\alpha^2 \sin\chi C_{Nw}(\lambda) \end{cases} \tag{26}$$

In Eq. (26), λ is wave wavelength, χ is wave encounter angle, ρ is sea water density, α is wave amplitude, L is ship length, $C_{Xw}(\lambda)$、$C_{Yw}(\lambda)$ and $C_{Nw}(\lambda)$) are wave drift force (moment) coefficients respectively.

Table 1
Yupeng Ship parameters.

Ship parameters	Value	Unit
Ship length L	189	m
Ship width B	27.8	m
draft d	11	m
Distance from center of gravity to center x_c	−0.18	m
Block coefficient C_b	0.72	C_b
Full load displacement	42293	t
Speed V	7.2	kn
Rudder blade area A_R	38	m^2
Turning ability index K	0.38	\
Turning lag index T	297.75	\

4.1. Comparative experiment for position prediction

In this part, the position prediction strategy will be compared with the no position prediction strategy, and some interesting conclusions can be obtained. In this experience, the following waypoint are showing in Tables 2 and 3. The parameters of the controller are:$c_1 = \pi/4$,$c_0 = 0.003$; $P = 1$,$Q = 0.1$; $k_1 = 1.2$, $k_2 = 0.48$, $k_3 = 0.64$; $K_p = 0.1$, $K_d = 5$; Ship initial velocity (u, v, r) = (7.2 m/s,0,0) , initial position coordinate (x, y) = (0,100m) . External disturbances: wind speed: 10 m/s; wind direction: 30sin (0.02t) + 45; velocity:1.0 m/s; flow direction: 10sin (0.005t) + 45; wave wavelength: 83 m; wave encounter angle:135°–30°sin(0.02t).The simulation results are shown in Fig. 4 and Fig. 5.

In Fig. 5, P1 is the path following situation of Euler method combine with ADRC, the prediction time domain n takes 40, P2 is the path following situation of ADRC, the prediction time domain n takes 0. Pd is the straight-line distance between two points and is also the reference path. Both algorithms can track the reference waypoint well. However, it is obvious that the future path prediction based on Euler method can greatly reduce the overshoot in the process of path following, and there is a great degree of overshoot when tracking the next waypoint in the process of path tracking based on prediction. Fig. 6 shows the path deviation of the two algorithms. Since the length of Yupeng vessel is 189m, the overshoot of ADRC algorithm does not exceed the length of ship, which is in line with the actual navigation. Through the Eulerian method to predict the future path, the maximum overshoot is no more than 30m, which greatly reduces the overshoot in the process of ship path following. It is shows that the algorithm proposed in this paper is effective.

5. 2Comparative experiment for ESO

On the basis of path prediction, this section compares the simulation results of power expended state observer (PESO) and liner expended state observer (LESO). The parameters of controller and observer unchanged. And the wind, wave, and currents remain unchanged, reselect the waypoint for following.

Fig. 7 shows the comparison of path following effects between LESO and PESO, where Y_1 is the path following effect based on LESO, and Y_2 is the path following effect based on PESO. Two observers both can well estimate the error, the path following effect of the two is basically the same, and both can well track the reference path. Moreover, because both use the Euler method to predict the future path, there is basically no

Table 2
Ship reference waypoint.

Desired waypoints	coordinates
Waypoint 1	(0,0)
Waypoint 2	(1000,0)
Waypoint 3	(3000,2000)
Waypoint 4	(6000,2000)
Waypoint 5	(8000,5000)
Waypoint 6	(19000,5000)

Table 3
Ship reference waypoint.

Desired waypoints	coordinates
Waypoint 1	(0,0)
Waypoint 2	(2000,0)
Waypoint 3	(4000,2000)
Waypoint 4	(8000,2000)
Waypoint 5	(10000,4000)
Waypoint 6	(14000,4000)

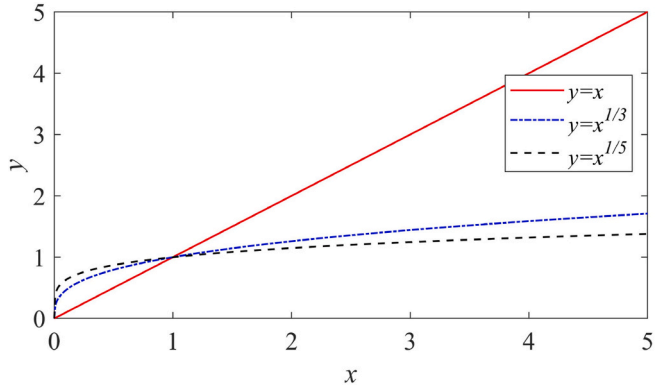

Fig. 4. Comparison between power function and linear function.

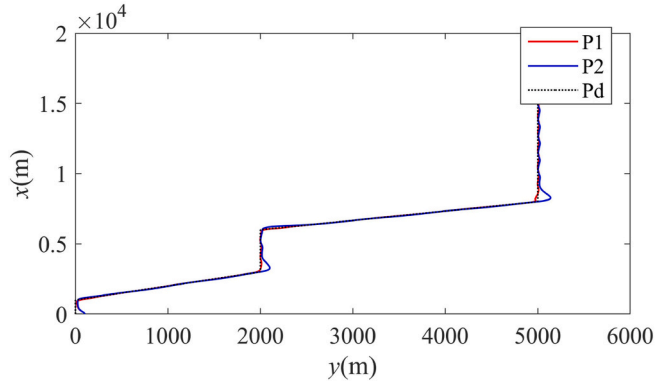

Fig. 5. Comparison of path following.

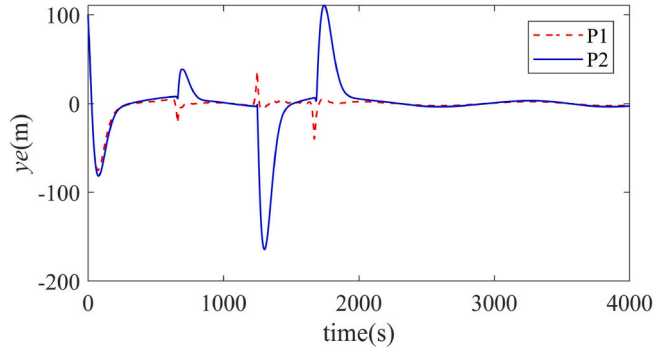

Fig. 6. Path following error comparison.

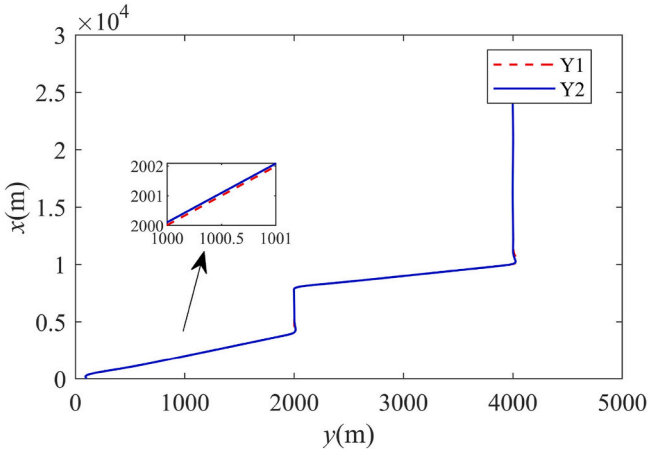

Fig. 7. Comparison of path following effect following between PESO and LESO.

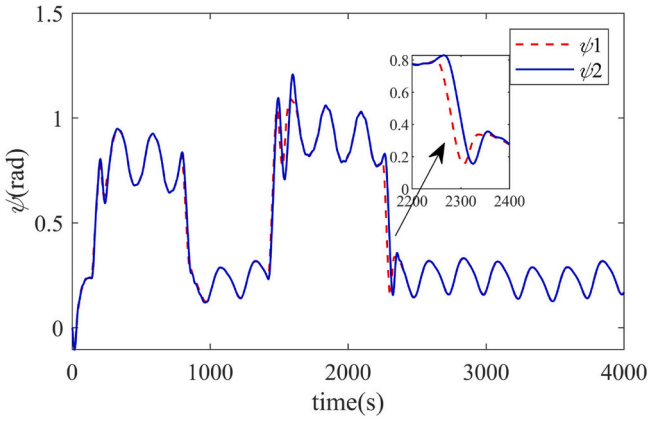

Fig. 8. Comparison of heading angle between LESO and PESO.

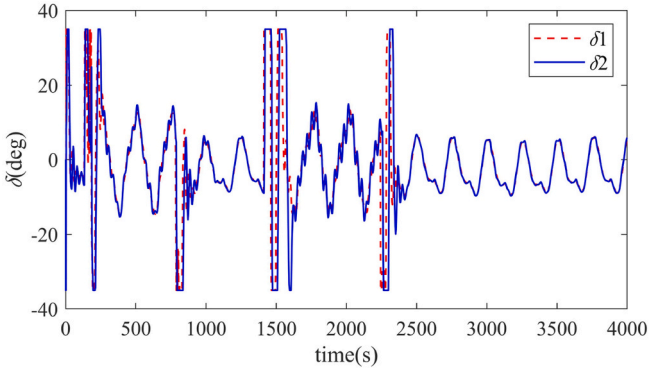

Fig. 9. Comparison of rudder angles between LESO and PESO.

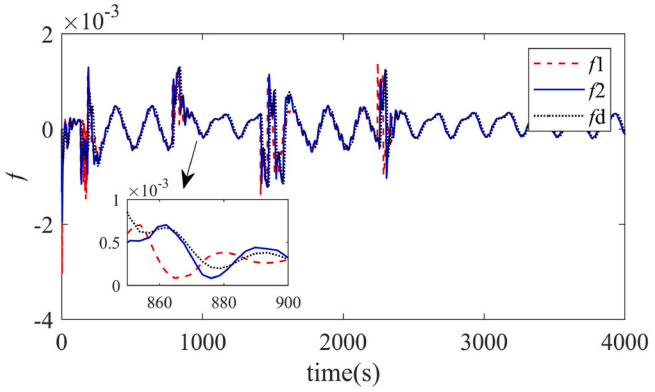

Fig. 10. Comparison of total disturbances f between LESO and PESO.

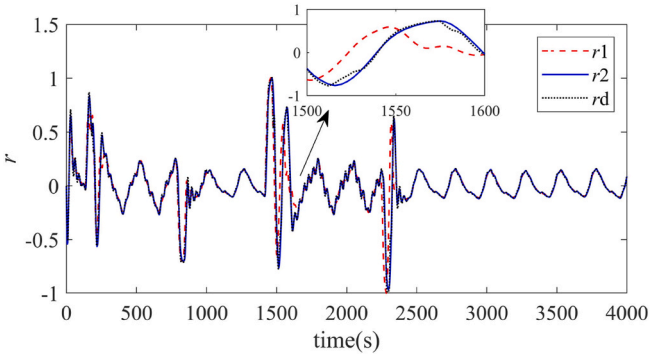

Fig. 11. Comparison of Yaw rate r between LESO and PESO.

overshoot. Fig. 8 shows the comparison of heading angle between LESO and PESO, ψ_1 is the change of heading angle based on LESO, and ψ_2 is the change of heading angle based on PESO. Due to the time-varying wind wave and currents disturbances, the heading angle oscillates slightly, but the heading tracking effect of both is very well. Fig. 9 is the comparison of rudder angle changes between PESO and LESO. δ_1 is the rudder angle change based on LESO, and δ_2 is the rudder angle change based on PESO. Similarly, due to the time-varying disturbance, regular oscillation occurs in the process of rudder angle change to reduce the effect of external disturbances on ship path following.

Fig. 10 and Fig. 11 show the estimation of total disturbances f and yaw rate r of LESO and PESO, respectively. In fact, f_1 and r_1 represent LESO's estimates of f and r, and f_2 and r_2 represent PESO's estimates of f and r. Both of them have well approximation effect. And PESO has larger gain when the error is small and smaller gain when the error is large, so it has better accuracy. In order to quantify the control effect, we define total estimation error f (*TEEF*) and total estimation error r (*TEER*)

$$\begin{cases} TEEF = \dfrac{1}{t_f - t_0}\displaystyle\int_{t_0}^{t_f} |f_e| \mathrm{dt} \\ TEER = \dfrac{1}{t_f - t_0}\displaystyle\int_{t_0}^{t_f} |r_e| \mathrm{dt} \end{cases} \tag{27}$$

It can be seen from Table 4 that the total disturbances f error based on LESO is 0.1806, but the total disturbances error based on PESO is only 0.1269, and the error of PESO is reduced by 43%. The total error of yaw angle based on LESO is 18.34°, while the total disturbances error based on PESO is only 14.81°, and the total error of PESO is reduced by 24%. It shows that the observer based on power function proposed in this paper has higher accuracy.

Table 4
Observer error.

Observer type	*TEEF*	*TEER*
LESO	0.1806	18.34
PESO	0.1269	14.81

6. Conclusion

In order to solve the problems of uncertain model, unknown external disturbances and overshoot in the process of ship path following, ADRC for ship path following combine with Euler method is proposed. The virtual heading angle is set by backstepping algorithm, and the three degree of freedom position control is transformed into one degree of freedom heading control. Due to the characteristics of large inertia and large time delay in ship path tracking, overshoot is easy to occur in the process of path following. Euler method is used to predict the future position in order to reduce overshoot. To solve the problems of internal model uncertainty and external wind and wave disturbances, the PESO is used to observe and compensate the total disturbances to the controller. Through the comparison of simulation experiments, compared with LESO, the estimation accuracy of PESO for f is improved by 43% and that for r is improved by 24%. And through the Euler method, the overshoot in the process of path following is greatly reduced, so that the maximum overshoot does not exceed 1/6 times the ship length. However, the computer simulation is only used in this paper, and no real ship simulation is adopted, our next study will consider the problem of ship path following in the case of a real ship.

CRediT authorship contribution statement

Hugan Zhang: Conceptualization, Methodology, Software, Validation, Formal analysis, Writing – original draft, Visualization. **Xianku Zhang:** Writing – original draft, Funding acquisition. **Tian Cao:** Writing – review & editing. **Renxiang Bu:** Supervision.

Declaration of competing interest

The authors declare that they have no known competing financial interests or personal relationships that could have appeared to influence the work reported in this paper.

Acknowledgements

Much appreciations to each reviewer for their valuable comments and suggestions to improve the quality of this note. This work is partially supported by the National Science Foundation of China (Grant No.51679024),Dalian Innovation Team Support Plan in the Key Research Field (2020RT08), The Fundamental Research Funds for the Central Universities") (3132021139).The authors would like to thank anonymous reviewers for their valuable comments to improve the quality of this article.

References

Chwa, D., 2021. Adaptive neural output feedback tracking control of underactuated ships against uncertainties in kinematics and system matrices. IEEE J. Ocean. Eng. 46, 720–735. https://doi.org/10.1109/JOE.2020.3024509.

Dai, S.-L., He, S., Wang, M., Yuan, C., 2019. Adaptive neural control of underactuated surface vessels with prescribed performance guarantees. IEEE Transact. Neural Networks Learn. Syst. 30, 3686–3698. https://doi.org/10.1109/TNNLS.2018.2876685.

Do, K.D., Pan, J., 2006. Robust path-following of underactuated ships: theory and experiments on a model ship. Ocean Eng. 33, 1354–1372. https://doi.org/10.1016/j.oceaneng.2005.07.011.

Esfahani, H.N., Szlapczynski, R., Ghaemi, H., 2019. High performance super-twisting sliding mode control for a maritime autonomous surface ship (MASS) using ADP-Based adaptive gains and time delay estimation. Ocean Eng. 191, 106526. https://doi.org/10.1016/j.oceaneng.2019.106526.

Gao, Zhiqiang, 2003. Scaling and bandwidth-parameterization based controller tuning. In: Proceedings of the 2003 American Control Conference, 2003. Presented at the 2003 American Control Conference. IEEE, Denver, CO, USA, pp. 4989–4996. https://doi.org/10.1109/ACC.2003.1242516.

Guan, W., Zhou, H., Su, Z., Zhang, X., Zhao, C., 2019. Ship steering control based on quantum neural network. Complexity 2019, 1–10. https://doi.org/10.1155/2019/3821048.

Guerrero, J., Torres, J., Creuze, V., Chemori, A., 2019. Trajectory tracking for autonomous underwater vehicle: an adaptive approach. Ocean Eng. 172, 511–522. https://doi.org/10.1016/j.oceaneng.2018.12.027.

Huang, H., Fan, Y., 2017. Path following for unmanned surface vessels based on adaptive LOS guidance and ADRC. In: Liu, D., Xie, S., Li, Y., Zhao, D., El-Alfy, E.-S.M. (Eds.), Neural Information Processing, Lecture Notes in Computer Science. Springer International Publishing, Cham, pp. 192–200. https://doi.org/10.1007/978-3-319-70136-3_21.

Kurtoglu, D., Bidikli, B., Tatlicioglu, E., Zergeroglu, E., 2021. Periodic disturbance estimation based adaptive robust control of marine vehicles. Ocean Eng. 219, 108351. https://doi.org/10.1016/j.oceaneng.2020.108351.

Le, T.T., 2021. Ship heading control system using neural network. J. Mar. Sci. Technol. 26, 963–972. https://doi.org/10.1007/s00773-020-00783-w.

Lekkas, A.M., Fossen, T.I., 2014. Integral LOS path following for curved paths based on a monotone cubic hermite spline parametrization. IEEE Trans. Control Syst. Technol. 22, 2287–2301. https://doi.org/10.1109/TCST.2014.2306774.

Li, R., Li, T., Bu, R., Zheng, Q., Chen, C.L.P., 2013. Active disturbance rejection with sliding mode control based course and path following for underactuated ships. Math. Probl Eng. 1–9. https://doi.org/10.1155/2013/743716, 2013.

Li, T., Zhao, R., Chen, C.L.P., Fang, L., Liu, C., 2018. Finite-time formation control of under-actuated ships using nonlinear sliding mode control. IEEE Trans. Cybern. 48, 3243–3253. https://doi.org/10.1109/TCYB.2018.2794968.

Li, Z., Li, R., Bu, R., 2020. Path following of under-actuated ships based on model predictive control with state observer. J. Mar. Sci. Technol. https://doi.org/10.1007/s00773-020-00746-1.

Liu, L., Wang, D., Peng, Z., Wang, H., 2016. Predictor-based LOS guidance law for path following of underactuated marine surface vehicles with sideslip compensation. Ocean Eng. 124, 340–348. https://doi.org/10.1016/j.oceaneng.2016.07.057.

Min, B., Zhang, X., 2021. Concise robust fuzzy nonlinear feedback track keeping control for ships using multi-technique improved LOS guidance. Ocean Eng. 224, 108734. https://doi.org/10.1016/j.oceaneng.2021.108734.

Mizuno, N., Saka, N., Katayama, T., 2016. A ship's automatic maneuvering system using optimal preview sliding mode controller with adaptation mechanism. IFAC-PapersOnLine 49, 576–581. https://doi.org/10.1016/j.ifacol.2016.10.497.

Moradi, M., Malekizade, H., 2013. Robust adaptive first–second-order sliding mode control to stabilize the uncertain fin-roll dynamic. Ocean Eng. 69, 18–23. https://doi.org/10.1016/j.oceaneng.2013.05.003.

Moreira, L., Fossen, T.I., Guedes Soares, C., 2007. Path following control system for a tanker ship model. Ocean Eng. 34, 2074–2085. https://doi.org/10.1016/j.oceaneng.2007.02.005.

Nguyen, Choi, Lee, 2019. Robust adaptive heading control for a ray-type hybrid underwater glider with propellers. JMSE 7, 363. https://doi.org/10.3390/jmse7100363.

Perera, L.P., Guedes Soares, C., 2012. Pre-filtered sliding mode control for nonlinear ship steering associated with disturbances. Ocean Eng. 51, 49–62. https://doi.org/10.1016/j.oceaneng.2012.04.014.

Shojaei, K., 2015. Leader–follower formation control of underactuated autonomous marine surface vehicles with limited torque. Ocean Eng. 105, 196–205. https://doi.org/10.1016/j.oceaneng.2015.06.026.

Sun, Z., 2017. Practical proportional integral sliding mode control for underactuated surface ships in the fields of marine practice. Ocean Eng. 7.

Wang, J., Zou, Z., Wang, T., 2018. Path following of a ship sailing in restricted waters based on an extended updated-gain high-gain observer. In: Ocean Engineering. Presented at the ASME 2018 37th International Conference on Ocean, Offshore and Arctic Engineering, vol. 7B. American Society of Mechanical Engineers, Madrid, Spain. https://doi.org/10.1115/OMAE2018-77795. V07BT06A030.

Wang, H., Tian, Y., Xu, H., 2021. Neural adaptive command filtered control for cooperative path following of multiple underactuated autonomous underwater vehicles along one path. IEEE Trans. Syst. Man Cybern, Syst. 1–13 https://doi.org/10.1109/TSMC.2021.3062077.

Xiaobin, Q., Yong, Y., Helong, S., Xiaofeng, S., Xiufeng, Z., 2016. Simulation system for testing ship dynamic positioning control algorithm. J. Syst. Simul. 28, 2028–2034.

Yang, H., Deng, F., He, Y., Jiao, D., Han, Z., 2020. Robust nonlinear model predictive control for reference tracking of dynamic positioning ships based on nonlinear disturbance observer. Ocean Eng. 215, 107885. https://doi.org/10.1016/j.oceaneng.2020.107885.

Yasukawa, H., Yoshimura, Y., 2015. Introduction of MMG standard method for ship maneuvering predictions. J. Mar. Sci. Technol. 20, 37–52. https://doi.org/10.1007/s00773-014-0293-y.

Zhang, G., Zhang, X., Zheng, Y., 2015. Adaptive neural path-following control for underactuated ships in fields of marine practice. Ocean Eng. 104, 558–567. https://doi.org/10.1016/j.oceaneng.2015.05.013.

Zhang, J., Xiang, X., Lapierre, L., Zhang, Q., Li, W., 2021c. Approach-angle-based three-dimensional indirect adaptive fuzzy path following of under-actuated AUV with input saturation. Appl. Ocean Res. 107, 102486. https://doi.org/10.1016/j.apor.2020.102486.

Zhang, H., Zhang, X., Bu, R., 2021a. Radial basis function neural network sliding mode control for ship path following based on position prediction. JMSE 9, 1055. https://doi.org/10.3390/jmse9101055.

Zhang, H., Zhang, X., Bu, R., 2021b. Active disturbance rejection control of ship course keeping based on nonlinear feedback and ZOH component. Ocean Eng. 233, 109136. https://doi.org/10.1016/j.oceaneng.2021.109136.

Zhang, Z., Zhang, X., Zhang, G., 2019. ANFIS-based course-keeping control for ships using nonlinear feedback technique. J. Mar. Sci. Technol. 24, 1326–1333. https://doi.org/10.1007/s00773-018-0581-z.

Zhao, H., Zhang, X., Han, X., 2019. Nonlinear control algorithms for efficiency-improved course keeping of large tankers under heavy sea state conditions. Ocean Eng. 189, 106371. https://doi.org/10.1016/j.oceaneng.2019.106371.

Zhu, G., Du, J., 2020. Global robust adaptive trajectory tracking control for surface ships under input saturation. IEEE J. Ocean. Eng. 45, 442–450. https://doi.org/10.1109/JOE.2018.2877895.

Zongxuan, L., Renxiang, B., Hugan, Z., 2021. Path following of ship based on sliding mode control with improved RBF neural network and virtual circle. J. Northwest. Polytech. Univ. 39, 216–223.